Robust Trajectory Tracking for Unmanned Aircraft Systems using a Nonsingular Terminal Modified Super-Twisting Sliding Mode Controller

Filiberto Muñoz, Eduardo Espinoza, Iván González-Hernández, Sergio Salazar, Rogelio Lozano

▶ **To cite this version:**

Filiberto Muñoz, Eduardo Espinoza, Iván González-Hernández, Sergio Salazar, Rogelio Lozano. Robust Trajectory Tracking for Unmanned Aircraft Systems using a Nonsingular Terminal Modified Super-Twisting Sliding Mode Controller. Journal of Intelligent and Robotic Systems, 2019, 93 (1-2), pp.55-72. 10.1007/s10846-018-0880-y . hal-01928186

HAL Id: hal-01928186
https://hal.science/hal-01928186

Submitted on 23 Nov 2023

HAL is a multi-disciplinary open access archive for the deposit and dissemination of scientific research documents, whether they are published or not. The documents may come from teaching and research institutions in France or abroad, or from public or private research centers.

L'archive ouverte pluridisciplinaire **HAL**, est destinée au dépôt et à la diffusion de documents scientifiques de niveau recherche, publiés ou non, émanant des établissements d'enseignement et de recherche français ou étrangers, des laboratoires publics ou privés.

Noname manuscript No.
(will be inserted by the editor)

Robust Trajectory Tracking for Unmanned Aircraft Systems Using a Nonsingular Terminal Modified Super-Twisting Sliding Mode Controller

Filiberto Muñoz · Eduardo S. Espinoza · Iván González · Sergio Salazar · Rogelio Lozano

Received: date / Accepted: date

Abstract The precision trajectory tracking problem for Unmanned Aerial Systems (UAS) is addressed in this work. A novel algorithm that combines a Nonsingular Modified Super-Twisting Controller with a High Order Sliding Mode Observer to enable an aerial vehicle tracking a desired trajectory under the assumption that i) its translational velocities are not available and ii) there are unmodeled dynamics and external disturbances. The proposed Sliding Mode Controller is based on a nonlinear sliding mode surface that ensures that the position and velocity tracking errors of all system's state variables converge to zero in finite time. Moreover, the proposed controller generates a continuous control signal eliminating the chattering phenomenon. Finally, simulation results and an extensive set of experiments are presented in order to illustrate the robustness and effectiveness of the proposed control strategy.

Keywords Nonsingular Terminal Modified Super Twisting · High Order Sliding Mode Observer · Unmanned Aerial System · RTK-GPS

F. Muñoz (⊠)
Autonomous Systems Laboratory, Mechatronics Department, Polytechnic University of Pachuca, Carretera Pachuca-Cd. Sahagun Km. 20, 43830, Zempoala, Hidalgo, México
Tel.: +52 771-547-7510 ext. 2223
E-mail: mupafi@upp.edu.mx

E. S. Espinoza − I. Gonzalez
Cátedras Conacyt. UMI LAFMIA, CINVESTAV-IPN, Av. IPN 2508, San Pedro Zacatenco C.P., 07360, Mexico D.F., México
E-mail: steedeq@gmail.com, igonzalez@ctrl.cinvestav.mx

S. Salazar − R. Lozano
UMI LAFMIA, CINVESTAV-IPN, Av. IPN 2508, San Pedro Zacatenco C.P., 07360, Mexico City., México
E-mail: sergio.salazar.cruz@gmail.com, rlozano@hds.utc.fr

R. Lozano
UTC-HEUDIASyC, Centre de Recherches de Royallieu, 60205, Compiegne, France
E-mail: rlozano@hds.utc.fr

1 Introduction

The growing interest for Quadrotor aircraft development has been accelerated during the last decade, mainly due to the advantages over comparable Vertical Take Off and Landing (VTOL) UASs, such as helicopters. A Quadrotor aircraft has simple hardware structure combined with inexpensive and reliable sensors. Applications of multirotors range from surveillance, aerial photograph, precision agriculture, search and rescue, to acrobatic maneouvers for entertaining. Nowadays, the applications and use of UASs is increasing exponentially but, simultaneously, the challenges related to improving its performance are also increasing, especially in the field of precision navigation.

With the main objective of find a satisfactory performance of Quadrotor vehicles, different control strategies have been proposed, such as Robust Controllers based on Sliding Mode techniques. Sliding Mode Control has been widely explored in unmanned systems due to the property of insensitivity to parametric uncertainties, model uncertainties and external disturbances [1], [2]. Control strategies based on First Order Sliding Modes have shown to be an effective method for controlling dynamic systems with uncertainties, unfortunately, these First Order strategies induce signals with chattering due to the discontinuous terms in the control law. In order to overcome these drawbacks, techniques known as Higher Order Sliding Modes Control have been developed [3]-[5]. These High Order strategies have improved the controllers' performance with respect to chattering effects.

The Second Order Super-Twisting Controller has been the most popular High Order Sliding Mode Controller used for controlling Quadrotor aircrafts, see for example [6]-[13]. In order to improve the convergence of the sliding variable in the Super Twisting algorithm, two linear correction terms are added to the classical Super Twisting to accelerate the approach of the sliding variable to the sliding surface. These modifications have been reported in [14]-[17]. The Sliding Mode Controllers based on linear sliding mode surface can only guarantee that closed-loop systems converge to the equilibrium asymptotically. In order to force the state of the system to reach the equilibrium in finite time, a terminal sliding mode control has been proposed.

Comparing the sliding mode control with the linear sliding surface, the terminal sliding mode presents important properties such as finite-time convergence. Although finite-time convergence can be guaranteed employing this method, the discontinuous signal will lead to the chattering phenomena caused by the switching control. Moreover, the terminal sliding mode has a singularity problem, that is, the terminal sliding mode control signal requieres to be infinitely large to maintain the ideal motion in some areas of the state space [18]. In [19] a terminal sliding mode tracking control for a class of SISO uncertain nonlinear systems with unknown external disturbances is proposed. In [20] a modified terminal sliding mode is used for solving a fixed-time consensus tracking for second-order multi-agent system.

In order to overcome the classical singularity problem of the conventional terminal sliding mode, the nonsingular terminal sliding mode has been pro-

posed. Moreover, nonsingular terminal sliding mode has a better performance against the controllers based on linear sliding mode surfaces [21]-[24]. In [18] a nonsingular terminal sliding-mode control for nonlinear systems is presented. In [21] an adaptive nonsingular terminal mode controller is proposed for spacecraft attitude tracking. A Continuous nonsingular terminal sliding mode control for systems with mismatched disturbances is presented in [22]. The Nonsingular Terminal Sliding Mode Control of Uncertain Second-Order Nonlinear System was stuied in [23]. A Non-singular terminal sliding mode controller applied to an actuated exoskeleton was developed in[24].

In real applications, the performance of the UAVs could be affected by external perturbations. In order to overcome this drawback, many research work are devoted to deal with the estimation of perturbations. In this sense, sliding mode observers provide a robust and finite-time convergence observer, while, high-order sliding mode observers preserves the same performance than standard sliding mode but without the undesired chattering effect. In [25] author proposes an finite-time arbitrary-order robust differentiator using high-order sliding mode, this differentiator could be used like a robust observer. Authors in [26] use a feedback linearization-based controller with a high-order sliding mode observer for a Quadrotor helicopter, where the high-order sliding mode observer is employed as an observer and estimator of the effect of the external disturbances such as wind and noise. In [27] the authors proposed observers using high-order sliding mode for obtaining the reconstruction of the exact non-linear system even in presence of disturbances.

This work is motivated by the tracking control in finite time of an UAS type Quadrotor affected by external disturbances, unmodeled dynamics and partial measurement of the state. Compared with most of the existing sliding mode control methods employed to control a UAS type Quadrotor, the main contribution of this paper are summarized as follows:

- A novel algorithm using a Nonsingular Modified Super-Twisting Controller enable to an aerial vehicle to track a desired trajectory that force the tracking error to reach the zero equilibrium in finite time.
- An output feedback Nonsingular Modified Super-Twisting Controller based on a High Order Sliding Mode Observer is developed, for case that only the system output is available. Also, it is show that the tracking error converges to zero in finite-time with the Controller-Observer proposed. In addition, a continuous control signal is obtained with the proposed strategy.
- Practical implementation is conducted in outdoor environments using a high preceision RTK-GPS system to show the effectiveness of the control strategy proposed.

The remainder of the paper is organized as follows. The dynamic model of the UAS type Quadrotor is presented in Section 2. The development of the Nonsingular Terminal Modified Super-Twisting Controller based on a High Order Sliding Mode Observer is showed in Section 3. The application of the Nonsingular Terminal Controller to the aerial vehicle is carry out in Section 4. A set of simulation and experimental results to illustrate the performance

of the control strategie proposed is presented in Section 5, followed by some concluding remarks in Section 6.

2 Dynamic Model

The quadrotor is an underactuated four-rotor unmanned aerial vehicle having six degrees of freedom and four control inputs including the total thrust and three angular moments. It has four rotors arranged in a cross shape. The front and rear motors rotate counterclockwise (CCW), while the other two motors rotate clockwise (CW). The main thrust is the sum of the thrusts of each motor, the pitch torque is a function of the difference $f_1 - f_3$, the roll torque is produced by the difference $f_2 - f_4$, and the yaw torque is the sum of $\tau_{M_1} + \tau_{M_2} + \tau_{M_3} + \tau_{M_4}$ (see Figure 1), where τ_{M_i} is the reaction torque of motor i due to shaft acceleration and the blades drag. Let $\Gamma_I = \{i_I, j_I, k_I\}$ be the inertial frame, $\Gamma_B = \{i_B, j_B, k_B\}$ denotes a set of coordinates fixed to the rigid aircraft.

Let $q = (x, y, z, \phi, \theta, \psi)^T \in \mathbb{R}^6 = (\zeta, \eta)^T$ be the generalized coordinates vector which describes the position and orientation of the flying machine, so the model could be separated in two coordinate subsystems: translational and rotational. These are defined respectively by

- $\zeta = (x, y, z)^T \in \mathbb{R}^3$: denotes the position of the aerial vehicle's center of mass relative to the inertial frame Γ_I.
- $\eta = (\phi, \theta, \psi)^T \in \mathbb{R}^3$: describe the orientation of the aerial vehicle and (ϕ,θ,ψ) are the three Euler angles: roll, pitch and yaw, respectively. These angles are bounded as follows: roll angle by ($-\pi/2 < \phi < \pi/2$), pitch angle by ($-\pi/2 < \theta < \pi/2$) and yaw angle by ($-\pi < \psi < \pi$).

Fig. 1: *Inertial* and *Body* frame of the mini Quadrotor aircraft.

The dynamic model is obtained using the Euler-Lagrange approach. We can decompose the equations into translational and rotational displacement. The Lagrangian of the aerial vehicle is given by the following equation

$$L(q, \dot{q}) = (T_{trasl} + T_{rot}) - U,$$

where

– T_{trasl}: Is the translational kinetic energy of the quad-rotor

$$T_{trasl} = \frac{1}{2} m \dot{\zeta}^T \dot{\zeta}.$$

– T_{rot}: Is the rotational kinetic energy of the quad-rotor

$$T_{rot} = \frac{1}{2} \dot{\eta}^T \mathbb{J} \dot{\eta}.$$

– U: Is the potential energy of the quad-rotor

$$U = mgz.$$

In compact form, the dynamic model of the Quadrotor is given as:

$$\begin{aligned} m\ddot{\zeta} &= F_I + mg \\ \mathbb{J}\ddot{\eta} &= \tilde{\tau}_\eta + C(\eta, \dot{\eta})\dot{\eta}. \end{aligned}$$

Afterwards, doing a change of coordinates, we propose new variables to the control input $\tilde{\tau}_\eta$:

$$\tau = \begin{pmatrix} \tau_\phi \\ \tau_\theta \\ \tau_\psi \end{pmatrix} = \mathbb{J}^{-1} \left(\tilde{\tau}_\eta - C\left(\eta, \dot{\eta}\right) \dot{\eta} \right),$$

where F_B can be expressed in the inertial frame F_I as $F_I = R^{B \to I} F^B$, $R^{B \to I}$ represents the rotation matrix which is defined by

$$R^{B \to I} = \begin{bmatrix} c\psi c\theta & c\psi s\theta - s\psi c\phi s\phi & c\psi s\theta c\phi + s\psi s\phi \\ s\psi c\theta & s\psi s\theta s\phi + c\psi c\phi & s\psi s\theta c\phi - c\psi s\phi \\ -s\theta & c\theta s\phi & c\theta c\phi \end{bmatrix},$$

where $s(\cdot) = sin(\cdot)$ and $c(\cdot) = cos(\cdot)$.

Finally, the dynamic model of the quadrotor can be described by the following equations:

$$\ddot{x} = \frac{1}{m}\left(\cos\phi\sin\theta\cos\psi + \sin\phi\sin\psi\right)u_1 - \frac{d_1}{m}\dot{x} \tag{1a}$$

$$\ddot{y} = \frac{1}{m}\left(\cos\phi\sin\theta\sin\psi - \sin\phi\cos\psi\right)u_1 - \frac{d_2}{m}\dot{y} \tag{1b}$$

$$\ddot{z} = \frac{1}{m}\left(\cos\phi\cos\theta\right)u_1 - g - \frac{d_3}{m}\dot{z} \tag{1c}$$

$$\ddot{\phi} = \dot{\theta}\dot{\psi}\frac{I_y - I_z}{I_x} - \frac{ld_4}{I_x}\dot{\phi} + \frac{l}{I_x}u_2 \tag{1d}$$

$$\ddot{\theta} = \dot{\phi}\dot{\psi}\frac{I_z - I_x}{I_y} - \frac{ld_5}{I_y}\dot{\theta} + \frac{l}{I_y}u_3 \tag{1e}$$

$$\ddot{\psi} = \dot{\phi}\dot{\theta}\frac{I_x - I_y}{I_z} - \frac{d_6}{I_z}\dot{\psi} + \frac{1}{I_z}u_4, \tag{1f}$$

where x, y, and z represent the Quadrotor's translational position in axis X, Y and Z, respectively. The translational velocities and translational accelerations are represented as $(\dot{x},\, \dot{y},\, \dot{z})$ and $(\ddot{x},\, \ddot{y},\, \ddot{z})$, respectively. The Euler angles roll, pitch and yaw are represented by ϕ, θ and ψ, respectively. The rotational velocities and rotational accelerations are given by $\left(\dot{\phi},\, \dot{\theta},\, \dot{\psi}\right)$ and $\left(\ddot{\phi},\, \ddot{\theta},\, \ddot{\psi}\right)$, respectively. The mass of the vehicle is denoted by m, the term g represents acceleration due to gravity, l is the distance of center of mass to the motors. The inertia moments of the vehicle are represented by I_x, I_y and I_z. The control inputs are given by $u_i,\ i = 1, \ldots, 4$. The terms $d_i,\ i = 1 \ldots 6$, represent drag coefficients.

3 Nonsingular Terminal Modified Super Twisting Controller Based on a High Order Sliding Mode Observer

In this section we present the mathematical structure of the Nonsingular Terminal Modified Super-Twisting Sliding Mode Controller and the High Order Sliding Mode Observer, which are the base for the Controller-Observer proposed in this work.

Consider a second order dynamic system defined as

$$\begin{aligned} \dot{\chi}_1(t) &= \chi_2(t) \\ \dot{\chi}_2(t) &= f(\chi(t)) + h(\chi(t))\,u(t) + \xi(t,\chi) \\ y(t) &= \chi_1(t), \end{aligned} \tag{2}$$

where $\chi(t) = [\chi_1(t),\, \chi_2(t)]^T \in \mathbb{R}^2$ represents the state vector, $y(t) \in \mathbb{R}$ is the system output, $u(t)$ is the input control signal, $f(\chi(t)) \in \mathbb{R}$ and $h(\chi(t)) \in \mathbb{R}$ are known functions. Moreover, the term $\xi(t,\chi) \in \mathbb{R}$ includes both unmodeled dynamics as external disturbances. We assume that disturbance $\xi(t,\chi)$ is Lipschitz and satisfies $|\dot{\xi}(t,\xi)| < \xi^+$ for a positive constant ξ^+. Hereafter, temporal dependence of the t variable will be omitted for simplicity.

3.1 High Order Sliding Mode Observer

The High Order Sliding Mode Observer used to estimate the dynamic χ_2 as well as the disturbance ξ of system (2) is given as

$$\begin{aligned}\dot{\hat{\chi}}_1 =&\hat{\chi}_2 + \lambda_1|\tilde{\chi}_1|^{\frac{2}{3}}\text{sign}\left(\tilde{\chi}_1\right)\\ \dot{\hat{\chi}}_2 =&\hat{\chi}_3 + \lambda_2|\tilde{\chi}_1|^{\frac{1}{3}}\text{sign}\left(\tilde{\chi}_1\right) + f\left(\chi\right) + h\left(\chi\right)u\\ \dot{\hat{\chi}}_3 =&\lambda_3\text{sign}\left(\tilde{\chi}_1\right),\end{aligned} \tag{3}$$

where $\hat{\chi}_i$, $i = 1, \ldots, 3$, represent the estimated variables. In the subsequent, variables with symbol $\hat{}$ denote estimated variables. The estimation errors are defined as $\tilde{\chi}_1 = \chi_1 - \hat{\chi}_1$, $\tilde{\chi}_2 = x_2 - \hat{\chi}_2$ and $\tilde{\chi}_3 = -\hat{\chi}_3 + \xi$. In the subsequent, variables with symbol $\tilde{}$ denote estimation error variables. Now, from (2) and (3), we can write the estimation error's dynamics as

$$\begin{aligned}\dot{\tilde{\chi}}_1 =& -\lambda_1|\tilde{\chi}_1|^{\frac{2}{3}}\text{sign}\left(\tilde{\chi}_1\right) + \tilde{\chi}_2\\ \dot{\tilde{\chi}}_2 =& -\lambda_2|\tilde{\chi}_1|^{\frac{1}{3}}\text{sign}\left(\tilde{\chi}_1\right) + \tilde{\chi}_3\\ \dot{\tilde{\chi}}_3 =& -\lambda_3\text{sign}\left(\tilde{\chi}_1\right) + \dot{\xi}.\end{aligned} \tag{4}$$

The dynamics of the estimation error (4) have the form of the non-recursive exact robust differentiator presented in [25]. The convergence proofs for (4) have been obtained by geometric methods in [25], by using homogeneity properties in [28] and by using a quadratic and strict Lyapunov function in [29]. Therefore, the estimation errors $\tilde{\chi}_1$, $\tilde{\chi}_2$, and $\tilde{\chi}_3$ will converge to zero in a finite time $t \geq T_0$ if gains λ_1, λ_2, and λ_3 are chosen appropriately [25], [29]. From the error variables definition, after finite time $t \geq T_0$, it results that $\chi_1 = \hat{\chi}_1$, $\chi_2 = \hat{\chi}_2$ and $\hat{\chi}_3 = \xi$.

3.2 Nonsingular Terminal Modified Super-Twisting Sliding Mode Controller

It is well known that the main drawback of the First Order Sliding Mode Control is the chattering phenomenon that appears in the control law. As a solution for solving this issue, authors in [3] presented Second Order Sliding algorithms, such as the Twisting algorithm, where the idea of acting on the superior derivatives of the sliding variable was introduced. On the other hand, in the case of the Second Order Sliding Mode Control, the following condition should be verified

$$s\left(\chi\right) = \dot{s}\left(\chi\right) = 0,$$

where $s\left(\chi\right)$ represents the sliding variable. In the remainder of the article, the dependence of χ on the $s\left(\chi\right)$ sliding variable will be omitted. The Modified Super-Twisting Sliding Mode Controller is a Second Order Sliding Mode (SOSM) algorithm introduced firstly by [30], and variations of this algorithm have been presented in [16], [17], [31].

In the following subsections we introduce the tracking control scheme using the nonsingular terminal modified super-twisting sliding mode controller both for the case where all the state variables are available and when the state variables are measured only partially.

A) Nonsingular Terminal Modified Super-Twisting Sliding Mode Controller

A nonlinear dynamic sliding mode manifold for system (2) is defined as follows

$$s = e_2 + c_1 e_1 + c_2 \exp^{-\lambda t} e_1^{(1-2\beta)}, \tag{5}$$

where $c_1 > 0$, $c_2 > 0$, $\lambda > 0$ and $0 < \beta < 1$. The sliding mode manifold ($s = 0$) guarantees the finite-time convergence of the error e_1 via the following dynamic equation

$$e_2 = -c_1 e_1 - c_2 \exp^{-\lambda t} e_1^{(1-2\beta)},$$

where the tracking errors are defined as $e_1 = \chi_1 - {\chi_1}^d$ and $e_2 = \chi_2 - {\chi_2}^d$, and the signal references are defined as ${\chi_1}^d$ and ${\chi_2}^d$. The finite-time convergence of the sliding mode can be proved by the following theorem.

Theorem 1 *[23] For system* (2)*, considering the sliding manifold* (5)*, the tracking error* e_1 *will converge to zero in finite time if* $2\beta c_1 - \lambda > 0$ *and the finite convergence time is*

$$Ts \leq \frac{\ln\left(1 + \left(\exp^{2\beta c_1 t} V^{\beta}(0)/a_2\right)\right)}{2\beta c_1 - \lambda},$$

where

$$a_2 = \frac{2^{(1-\beta)}\beta c_1}{2\beta c_1 - \lambda} > 0 \quad \textit{and} \quad V = \frac{1}{2}e_1^2.$$

□

The temporal derivative of the sliding variable, with the dynamics of the system (2) is given as

$$\dot{s} = f(\chi) + h(\chi)\, u + \xi - \dot{\chi}_2^d + c_1 \dot{e}_1 + A, \tag{6}$$

with A defined as

$$A = c_2 \exp^{-\lambda t} e_1^{-2\beta} \left[(1 - 2\beta)\, \dot{e}_1 - \lambda e_1\right].$$

Proposition 1. Let the Nonsingular Terminal Modified Super Twisting control input u be defined as

$$\begin{aligned} u = & h(\chi)^{-1} \Big[-f(\chi) + \dot{\chi}_2^d - c_1 \dot{e}_1 - A + c_1 \dot{\chi}_1^d - k_1 |s|^{\frac{1}{2}} \operatorname{sign}(s) \\ & - k_2 s - \int_0^t k_3 \operatorname{sign}(s)\, d\tau - \int_0^t k_4 s d\tau \Big]. \end{aligned} \tag{7}$$

By properly selecting the gains k_1, k_2, k_3 and k_4, then $s = \dot{s} = 0$ in finite time, which implies that the tracking errors e_1 and e_2 will converge to zero in finite time.

Proof. Substituting the Nonsingular Terminal Modified Super Twisting Controller (7) in (6) we obtain

$$\dot{s} = -k_1|s|^{\frac{1}{2}}\text{sign}\,(s) - k_2 s - \int_0^t k_3\text{sign}\,(s)\,d\tau - \int_0^t k_4 s d\tau + \xi.$$

Defining new variables ω_1 and ω_2 as

$$\begin{aligned}\omega_1 =& s\\ \omega_2 =& -k_3\int_0^t \text{sign}\,(s)\,d\tau - k_4\int_0^t s d\tau + \xi,\end{aligned}$$

it can be obtained the following closed loop dynamic corresponding to the sliding surface

$$\begin{aligned}\dot{\omega}_1 =& -k_1|\omega_1|^{1/2}\text{sign}\,(\omega_1) - k_2\omega_1 + \omega_2\\ \dot{\omega}_2 =& -k_3\text{sign}\,(\omega_1) - k_4\omega_1 + \dot{\xi}.\end{aligned}$$

Suppose that for system (2) the derivative of the disturbance is globally bounded by $|\dot{\xi}| < \xi_1 + \xi_2|x_1|$ with $\xi_1 > 0$ and $\xi_2 > 0$, assuming that the gains k_1, k_2, k_3, k_4 are selected according to

$$\begin{aligned}k_1 &> \sqrt{\xi_1}\\ k_2 &> \frac{1}{2}\sqrt{8\xi_2}\\ k_3 &> \xi_1\\ k_4 &> \frac{k_1\left[\frac{1}{2}k_1^3\left(2k_2 - \xi_2\right) + \left(\frac{5}{2}k_2^2 + \xi_2\right)p_1\right]}{k_1\left(p_1 - \frac{1}{2}k_1^3\right)},\end{aligned}$$

where

$$p_1 = k_1\left(\frac{1}{4}k_1^2 - \xi_1\right) + \frac{1}{2}k_1\left(2k_3 + \frac{1}{2}k_1^2\right).$$

Then, the Nonsingular Terminal Modified Super Twisting Controller (7) yields finite-time convergence of the sliding surface $s = 0$ [29],[30] and from Theorem 1, the tracking errors e_1 and e_2 will converge to zero in finite time.

B) Nonsingular Terminal Modified Super-Twisting Sliding Mode Controller based on High Order Sliding Mode Observer

Assuming that the state variable χ_2 is unmeasured, the design of the Nonsingular Terminal Modified Super-Twisting Sliding Mode Controller will be based on the High Order Sliding Mode Observer presented in Subsection 3.1. In this sense, a nonlinear dynamic sliding mode manifold for system (2) by using the estimation $\hat{\chi}_2$ is defined as follows

$$s = \hat{e}_2 + c_1 e_1 + c_2\exp^{-\lambda t}e_1^{(1-2\beta)},$$

where the tracking error $\hat{e}_2$ is defined as $\hat{e}_2 = \hat{\chi}_2 - {\chi_2}^d$. The temporal derivative of the sliding variable, with the dynamics of the system (2) is given as

$$\dot{s} = \dot{\hat{e}}_2 + c_1\dot{e}_1 + c_2 \exp^{-\lambda t} e_1^{-2\beta} \left[(1-2\beta)\,\dot{e}_1 - \lambda e_1\right].$$

Substituting the dynamics of system (2) and observer (3) in the dynamics of the sliding manifold we obtain

$$\begin{aligned} \dot{s} = &\int_0^t \lambda_3 \text{sign}\left(\tilde{\chi}_1\right) d\tau + \lambda_2 |\tilde{\chi}_1|^{\frac{1}{3}} \text{sign}\left(\tilde{\chi}_1\right) + f\left(\chi\right) + h\left(\chi\right) u - \dot{x}_2^d + \\ & c_1\left(\tilde{\chi}_2 + \hat{\chi}_2 - \dot{x}_1^d\right) + c_2 \exp^{-\lambda t} e_1^{2\beta}\left[(1-2\beta)\left(\tilde{\chi}_2 + \hat{\chi}_2 - \dot{x}_1^d\right) - \lambda e_1\right]. \end{aligned} \tag{8}$$

Proposition 2. Let the Nonsingular Terminal Modified Super Twisting control input u based on High Order Sliding Mode Observer (3) be defined as

$$\begin{aligned} u = &h\left(\chi\right)^{-1}\left[-\int_0^t \lambda_3 \text{sign}\left(\tilde{\chi}_1\right) d\tau - \lambda_2 |\tilde{\chi}_1|^{\frac{1}{3}} \text{sign}\left(\tilde{\chi}_1\right) - f\left(\chi\right) + \dot{x}_2^d - c_1\hat{\chi}_2 \right. \\ & + c_1\dot{\chi}_1^d - c_2 \exp^{-\lambda t} e_1^{2\beta}\left[(1-2\beta)\left(\hat{\chi}_2 - \dot{\chi}_1^d\right) - \lambda e_1\right] - k_1 |s|^{\frac{1}{2}} \text{sign}\left(s\right) \\ & \left. -k_2 s - \int_0^t k_3 \text{sign}\left(s\right) d\tau - \int_0^t k_4 s d\tau - \hat{\chi}_3\right]. \end{aligned} \tag{9}$$

By properly selecting the gains k_1, k_2, k_3 and k_4, then $s = \dot{s} = 0$ in finite time, which implies that by Theorem 1 the tracking errors e_1 and e_2 will converge to zero in finite time.

Proof. Substituting the Nonsingular Terminal Modified Super Twisting Controller based on High Order Sliding Mode Observer (9) in (8) we obtain

$$\begin{aligned} \dot{s} = &c_1\tilde{\chi}_2 + c_2 \exp^{-\lambda t} e_1^{2\beta}\left[(1-2\beta)\,\tilde{\chi}_2\right] - k_1 |s|^{\frac{1}{2}} \text{sign}\left(s\right) - k_2 s \\ & - \int_0^t k_3 \text{sign}\left(s\right) d\tau - \int_0^t k_4 s d\tau + \xi - \hat{\chi}_3. \end{aligned}$$

Therefore, the closed-loop Controller-Observer system is given by the following expressions

$$\Gamma = \begin{cases} \dot{\chi}_1 = s - c_1 e_1 - c_2 \exp^{-\lambda t} e_1^{(1-2\beta)} + \tilde{\chi}_2 + {x_2}^d \\ \dot{s} = \tilde{\chi}_2\left(c_1 + c_2 \exp^{-\lambda t} e_1^{2\beta}\left(1-2\beta\right)\right) - k_1 |s|^{\frac{1}{2}} \text{sign}\left(s\right) \\ \qquad - k_2 s + \xi - \hat{\chi}_3 + v \\ \dot{v} = -k_3 \text{sign}\left(s\right) - k_4 s, \end{cases}$$

$$\Sigma = \begin{cases} \dot{\tilde{\chi}}_1 = -\lambda_1 |\tilde{\chi}_1|^{2/3} \text{sign}\left(\tilde{\chi}_1\right) + \tilde{\chi}_2 \\ \dot{\tilde{\chi}}_2 = -\lambda_2 |\tilde{\chi}_1|^{1/3} \text{sign}\left(\tilde{\chi}_1\right) + \tilde{\chi}_3 \\ \dot{\tilde{\chi}}_3 = -\lambda_3 \text{sign}\left(\tilde{\chi}_1\right) + \dot{\xi}. \end{cases} \tag{10}$$

The estimation error of observer (10) converges to zero in finite-time. Consequently, we obtain for the error variables that $\tilde{\chi}_1 = \tilde{\chi}_2 = \tilde{\chi}_3 = 0$. After time T_0, the closed-loop system is given by the dynamics

$$\Gamma = \begin{cases} \dot{\chi}_1 = s - c_1 e_1 - c_2 \exp^{-\lambda t} e_1^{(1-2\beta)} + {x_2}^d \\ \dot{s} = -k_1 |s|^{\frac{1}{2}} \text{sign}\,(s) - k_2 s + v \\ \dot{v} = -k_3 \text{sign}\,(s) - k_4 s. \end{cases} \tag{11}$$

The last two terms of (11) represent a Modified Super Twisting Sliding Mode Controller introduced in [30], where choosing the gains as

$$k_i > 0, \quad i = 1, \ldots, 4$$
$$4k_3k_4 > \left(8k_3 + 9k_1^2\right) k_2^2,$$

then it is obtained $s = \dot{s} = 0$ in finite time. This implies that the tracking errors e_1 and e_2 are asymptotically stable. Finally, we obtain that χ_1 and $\hat{\chi}_2$ converge in finite time to ${\chi_1}^d$ and ${\chi_2}^d$, respectively.

4 Robust Controller for the aerial vehicle

In this section, a robust controller for position and attitude tracking of the Quadrotor helicopter will be discussed. Position and attitude robust control are designed by considering a time-scale separation between the translational dynamics and the orientation dynamics. This approach is based on the assumption that the closed-loop attitude dynamics converge faster than the closed-loop translational dynamics [32], [33].

From (1) it can be seen that the Quadrotor dynamics can be divided into two subsystems: i) an underactuated system composed by dynamics $\ddot{x}, \ddot{y}, \ddot{\phi}, \ddot{\theta}$ and ii) a fully actuated system composed of dynamics $\ddot{z}$ and $\ddot{\psi}$.

Control Problem Formulation.

For the Quadrotor dynamics (1), it is necessary to design control inputs u_1, u_2, u_3 and u_4 using a Nonsingular Terminal Modified Super-Twisting Sliding Mode Controller, such that:

- The position and velocity tracking errors of all system state variables converge to zero in finite.
- For the fully actuated subsystem, it is required that yaw angle ψ and altitude z tracking robustly signals ψ^d and z^d.
- For underactuated subsystem controller, it is necessary to guarantee that positions x and y tracking robustly signals x^d and y^d, respectively, whilst ϕ and θ tracking robustly ϕ^{des} and θ^{des}.
- Desired references x^d, y^d, z^d and ψ^d are generated by a trajectory generator or an upper level controller, whereas references ϕ^{des} and θ^{des} are generated by using (1a) and (1b).

– Translational velocities $\dot{x}, \dot{y}, \dot{z}$ cannot be measured online, so they will be estimated by a High Order Sliding Mode Observer.

4.1 Position Control

The position controller generates the desired references for the pitch and roll angles ϕ^{des} and θ^{des}, respectively, and simultaneously, stabilizes the altitude of the Quadrotor.

Altitude Controller. From (1c), we can express the altitude dynamics as

$$\begin{aligned} \dot{z}_1 =& z_2 \\ \dot{z}_2 =& \frac{1}{m}\left(\cos\phi\cos\theta\right) u_1 - g + \xi_z, \end{aligned} \tag{12}$$

where $z_1 = z$ and $z_2 = \dot{z}$. In this work, we assume that the term $-\frac{d_3}{m}\dot{z}$ is treated as a unmodeled dynamic and it is included in the term ξ_z (external disturbances can also be included in ξ_z). In order to track a desired altitude ${z_1}^d$, we employ the Modified Super-Twisting Controller based on the High Order Sliding Mode Observer (3) presented in Section 3. The dynamics of observer (3) applied to the altitude dynamics (12) are given by

$$\begin{aligned} \dot{\hat{z}}_1 =& \hat{z}_2 + \lambda_{1z}|\tilde{z}_1|^{\frac{2}{3}}\mathrm{sign}\left(\tilde{z}_1\right) \\ \dot{\hat{z}}_2 =& \hat{z}_3 + \lambda_{2z}|\tilde{z}_1|^{\frac{1}{3}}\mathrm{sign}\left(\tilde{z}_1\right) + \frac{1}{m}\left(\cos\phi\cos\theta\right) u_1 - g \\ \dot{\hat{z}}_3 =& \lambda_{3z}\mathrm{sign}\left(\tilde{z}_1\right), \end{aligned} \tag{13}$$

where $\tilde{z}_1 = z_1 - \hat{z}_1$ is the observation error of z_1, $\hat{z}_1$ and $\hat{z}_2$ represent the altitude position and the estimated velocity, respectively. The term $\hat{z}_3$ is the estimated of the disturbance ξ_z. Let us define a nonlinear sliding manifold s_z as

$$s_z = \left(\hat{z}_2 - {z_2}^d\right) + c_{z_1}\left(z_1 - {z_1}^d\right) + c_{z_2}\exp^{-\lambda_z t}\left(z_1 - {z_1}^d\right)^{(1-2\beta_z)},$$

where $c_{z_1} > 0$, $c_{z_2} > 0$, $\lambda_z > 0$ and $0 < \beta_z < 1$. The control signal u_1 is given by

$$\begin{aligned} u_1 =& \frac{m}{\cos\phi\cos\theta}\left[-\int_0^t \lambda_{3z}\mathrm{sign}\left(\tilde{z}_1\right)d\tau - \lambda_{2z}|\tilde{z}_1|^{\frac{1}{3}}\mathrm{sign}\left(\tilde{z}_1\right) + g + \dot{z}_2^d - c_{z_1}\hat{z}_2\right. \\ &+ c_{z_1}\dot{z}_1^d - c_{z_2}\exp^{-\lambda_z t}\left(z_1 - {z_1}^d\right)^{2\beta_z}\left[(1-2\beta_z)\left(\hat{z}_2 - \dot{z}_1^d\right) - \lambda_z\left(z_1 - {z_1}^d\right)\right] \\ &\left. -k_{1z}|s_z|^{\frac{1}{2}}\mathrm{sign}\left(s_z\right) - k_{2z}s_z - \int_0^t k_{3z}\mathrm{sign}\left(s_z\right)d\tau - \int_0^t k_{4z}s_z d\tau\right]. \end{aligned} \tag{14}$$

Combining controller (14) together with observer (13), ensures that z_1 tracks in finite time to ${z_1}^d$ under unknown disturbances and estimating on line the altitude velocity z_2.

Horizontal Controller. The Quadrotor's translational dynamics in X axis represented by (1a) can be rewritten as

$$\begin{aligned}\dot{x}_1 =& x_2\\ \dot{x}_2 =& \mu_x + \xi_x,\end{aligned}$$

where $\mu_x = \frac{1}{m}\left(\cos\phi\sin\theta\cos\psi + \sin\phi\sin\psi\right)u_1$ and $\xi_x = -\frac{d_1}{m}\dot{x}$ (this term can also include external disturbances). Defining μ_{x_v} as a new *virtual* control input, to track the desired position ${x_1}^d$, the following sliding variable is defined

$$s_x = \left(\hat{x}_2 - {x_2}^d\right) + c_{x_1}\left(x_1 - {x_1}^d\right) + c_{x_2}\exp^{-\lambda_x t}\left(x_1 - {x_1}^d\right)^{(1-2\beta_x)},$$

where $c_{x_1} > 0$, $c_{x_2} > 0$, $\lambda_x > 0$ and $0 < \beta_x < 1$. The virtual control input μ_{x_v} is given as

$$\begin{aligned}\mu_{x_v} = \Bigg[&-\int_0^t \lambda_{3x}\mathrm{sign}\left(\tilde{x}_1\right)d\tau - \lambda_{2x}|\tilde{x}_1|^{\frac{1}{3}}\mathrm{sign}\left(\tilde{x}_1\right) + \dot{x}_2^d - c_{x_1}\hat{x}_2 + c_{x_1}\dot{x}_1^d\\ &- c_{x_2}\exp^{-\lambda_x t}\left(x_1 - {x_1}^d\right)^{2\beta_x}\left[(1-2\beta_x)\left(\hat{x}_2 - \dot{x}_1^d\right) - \lambda_x\left(x_1 - {x_1}^d\right)\right]\\ &-k_{1x}|s_x|^{\frac{1}{2}}\mathrm{sign}\left(s_x\right) - k_{2x}s_x - \int_0^t k_{3x}\mathrm{sign}\left(s_x\right)d\tau - \int_0^t k_{4x}s_x d\tau\Bigg].\end{aligned} \tag{15}$$

Following the same procedure, for the dynamic in Y axis, defining $\mu_y = \frac{1}{m}\left(\cos\phi\sin\theta\sin\psi - \sin\phi\cos\psi\right)u_1$ and $\xi_y = -\frac{d_2}{m}\dot{y}$. The dynamics given in (1b) can be rewritten as

$$\begin{aligned}\dot{y}_1 =& y_2\\ \dot{y}_2 =& \mu_y + \xi_y,\end{aligned}$$

the sliding variable s_y is proposed as

$$s_y = \left(\hat{y}_2 - {y_2}^d\right) + c_{y_1}\left(y_1 - {y_1}^d\right) + c_{y_2}\exp^{-\lambda_y t}\left(y_1 - {y_1}^d\right)^{(1-2\beta_y)},$$

where $c_{y_1} > 0$, $c_{y_2} > 0$, $\lambda_y > 0$ and $0 < \beta_y < 1$. The virtual control input μ_{y_v} is given as

$$\begin{aligned}\mu_{y_v} = \Bigg[&-\int_0^t \lambda_{3y}\mathrm{sign}\left(\tilde{y}_1\right)d\tau - \lambda_{2y}|\tilde{y}_1|^{\frac{1}{3}}\mathrm{sign}\left(\tilde{y}_1\right) + \dot{y}_2^d - c_{y_1}\hat{y}_2 + c_{y_1}\dot{y}_1^d\\ &- c_{y_2}\exp^{-\lambda_y t}\left(y_1 - {y_1}^d\right)^{2\beta_y}\left[(1-2\beta_y)\left(\hat{y}_2 - \dot{y}_1^d\right) - \lambda_y\left(y_1 - {y_1}^d\right)\right]\\ &-k_{1y}|s_y|^{\frac{1}{2}}\mathrm{sign}\left(s_y\right) - k_{2y}s_y - \int_0^t k_{3y}\mathrm{sign}\left(s_y\right)d\tau - \int_0^t k_{4y}s_y d\tau\Bigg].\end{aligned} \tag{16}$$

Virtual controllers (15) and (16) combined with High Order Sliding Mode Observer (3), guarantee that x_1 and y_1 tracks in finite time to ${x_1}^d$ and ${y_1}^d$, respectively.

In order to force the virtual controllers to match μ_x and μ_y, i. e. $\mu_{x_v} = \mu_x$ and $\mu_{y_v} = \mu_y$, it is necessary to obtain a relation between the virtual controllers and the angles ϕ and θ. Based on (1a) and (1b), we obtain the following expressions

$$\mu_{x_v} \cos\psi = \frac{1}{m}\left(\cos\phi \sin\theta \cos^2\psi + \sin\phi \cos\psi \sin\psi\right) u_1 + \cos\psi\, \xi_x$$
$$\mu_{y_v} \sin\psi = \frac{1}{m}\left(\cos\phi \sin\theta \sin^2\psi - \sin\phi \cos\psi \sin\psi\right) u_1 + \sin\psi\, \xi_y.$$

The desired angles ϕ^{des} and θ^{des} (in function of virtual controllers μ_{x_v} and μ_{y_v} given by (15) and (16), respectively) that enables the system to track desired positions ${x_1}^d$ and ${y_1}^d$ are given as

$$\phi^{des} = \arcsin\left(\frac{m\left[\sin\psi^d\, \mu_{x_v} - \cos\psi^d\, \mu_{y_v}\right]}{u_1} - \frac{\sin\psi^d\, \xi_{x_v} - \cos\psi^d\, \xi_{y_v}}{u_1}\right)$$
$$\theta^{des} = \arcsin\left(\frac{m\left[\cos\psi^d\, \mu_{x_v} - \sin\psi^d\, \mu_{y_v}\right]}{u_1 \cos\phi^{des}} - \frac{\cos\psi^d\, \xi_{x_v} + \sin\psi^d\, \xi_{y_v}}{u_1 \cos\phi^{des}}\right).$$

It is worth mentioning that the disturbance terms ξ_x and ξ_y will be estimated by using the High Order Sliding Mode Observer.

4.2 Attitude Control

To develop the controller for the attitude subsystem, we express (1d)-(1f) as

$$\ddot{\phi} = \frac{l}{I_x} u_2 + \xi_\phi$$
$$\ddot{\theta} = \frac{l}{I_y} u_3 + \xi_\theta$$
$$\ddot{\psi} = \frac{1}{I_z} u_4 + \xi_\psi,$$

where $\xi_\phi = \dot{\theta}\dot{\psi}\frac{I_y - I_z}{I_x} - \frac{l d_4}{I_x}\dot{\phi}$, $\xi_\theta = \dot{\phi}\dot{\psi}\frac{I_z - I_x}{I_y} - \frac{l d_5}{I_y}\dot{\theta}$ and $\xi_\psi = \dot{\phi}\dot{\theta}\frac{I_x - I_y}{I_z} - \frac{d_6}{I_z}\dot{\psi}$. The attitude controller for the Quadrotor is developed using the Nonsingular Terminal Modified Super-Twisting Control, which enables the system to follow the desired orientation given by angles ϕ^{des}, θ^{des} and ψ^d. To accomplish this task, the following sliding manifolds are defined as

$$s_\phi = \left(\phi_2 - {\phi_2}^{des}\right) + c_{\phi_1}\left(\phi_1 - {\phi_1}^{des}\right) + c_{\phi_2}\exp^{-\lambda_\phi t}\left(\phi_1 - {\phi_1}^{des}\right)^{(1-2\beta_\phi)}$$
$$s_\theta = \left(\theta_2 - {\theta_2}^{des}\right) + c_{\theta_1}\left(\theta_1 - {\theta_1}^{des}\right) + c_{\theta_2}\exp^{-\lambda_\theta t}\left(\theta_1 - {\theta_1}^{des}\right)^{(1-2\beta_\theta)}$$
$$s_\psi = \left(\psi_2 - {\psi_2}^{des}\right) + c_{\psi_1}\left(\psi_1 - {\psi_1}^{des}\right) + c_{\psi_2}\exp^{-\lambda_\psi t}\left(\psi_1 - {\psi_1}^{des}\right)^{(1-2\beta_\psi)},$$

where $\phi_1 = \phi$, $\phi_2 = \dot{\phi}$, $\theta_1 = \theta$, $\theta_1 = \dot{\theta}$, $\psi_1 = \psi$ and $\psi_2 = \dot{\psi}$, the gains c_{ϕ_1}, c_{ϕ_2}, c_{θ_1}, c_{θ_2}, c_{ψ_1}, c_{ψ_2} are positive, and $0 < \beta_\phi < 1$, $0 < \beta_\theta < 1$, $0 < \beta_\psi < 1$.

Based on the assumption that the orientation velocities are available, the following controllers are proposed for Quadrotor's attitude

$$\begin{aligned} u_2 =& \frac{I_x}{l}\left[-c_{\phi_2}\exp^{-\lambda_\phi t}\left(\phi_1-{\phi_1}^{des}\right)^{-2\beta_\phi}\left\{(1-2\beta_\phi)\left(\phi_2-{\phi_2}^{des}\right)\right.\right. \\ & \left.-\lambda_\phi\left(\phi_1-{\phi_1}^{des}\right)\right\}-\dot{\theta}\dot{\psi}\frac{I_y-I_z}{I_x}+\dot{\phi}_2^{des}-c_{\phi_1}\phi_2+c_{\phi_1}\dot{\phi}_1^{des} \\ & \left.-k_{1\phi}|s_\phi|^{\frac{1}{2}}\mathrm{sign}\left(s_\phi\right)-k_{2\phi}s_\phi-\int_0^t k_{3\phi}\mathrm{sign}\left(s_\phi\right)d\tau-\int_0^t k_{4\phi}s_\phi d\tau\right], \end{aligned} \tag{17}$$

$$\begin{aligned} u_3 =& \frac{I_x}{l}\left[-c_{\theta_2}\exp^{-\lambda_\theta t}\left(\theta_1-{\theta_1}^{des}\right)^{-2\beta_\theta}\left\{(1-2\beta_\theta)\left(\theta_2-{\theta_2}^{des}\right)\right.\right. \\ & \left.-\lambda_\theta\left(\theta_1-{\theta_1}^{des}\right)\right\}-\dot{\theta}\dot{\psi}\frac{I_y-I_z}{I_x}+\dot{\theta}_2^{des}-c_{\theta_1}\theta_2+c_{\theta_1}\dot{\theta}_1^{des} \\ & \left.-k_{1\theta}|s_\theta|^{\frac{1}{2}}\mathrm{sign}\left(s_\theta\right)-k_{2\theta}s_\theta-\int_0^t k_{3\theta}\mathrm{sign}\left(s_\theta\right)d\tau-\int_0^t k_{4\theta}s_\theta d\tau\right], \end{aligned} \tag{18}$$

$$\begin{aligned} u_4 =& \frac{I_x}{l}\left[-c_{\psi_2}\exp^{-\lambda_\psi t}\left(\psi_1-{\psi_1}^{des}\right)^{-2\beta_\psi}\left\{(1-2\beta_\psi)\left(\psi_2-{\psi_2}^{des}\right)\right.\right. \\ & \left.-\lambda_\psi\left(\psi_1-{\psi_1}^{des}\right)\right\}-\dot{\psi}\dot{\psi}\frac{I_y-I_z}{I_x}+\dot{\psi}_2^{des}-c_{\psi_1}\psi_2+c_{\psi_1}\dot{\psi}_1^{des} \\ & \left.-k_{1\psi}|s_\psi|^{\frac{1}{2}}\mathrm{sign}\left(s_\psi\right)-k_{2\psi}s_\psi-\int_0^t k_{3\psi}\mathrm{sign}\left(s_\psi\right)d\tau-\int_0^t k_{4\psi}s_\psi d\tau\right]. \end{aligned} \tag{19}$$

5 Simulation and Experimental Results

In order to show the right performance of the control strategies proposed, a set of simulation as well as experimental results carry out in outdoor environments is presented in this section.

5.1 Simulation Results

We present a set of simulation results where a square trajectory of 10 meters is tracked by the Quadrotor aircraft. The control laws (14),(15),(16),(17)-(19) together with observer (3) are applied to the system given by Equation (1). The Quadrotor parameters considered in the simulation test are given in Table I. Table II and Table III present the parameters employed for the Modified

Table 1: Quadrotor model parameters.

Parameter	Value	Unit
m	0.8	kg
l	0.2	m
g	9.81	m/s^2
$I_x = I_y$	0.0075	Ns^2/rad
I_z	0.013	Ns^2/rad
$k_1 = k_2 = k_3$	0.01	Ns/m
$k_4 = k_5 = k_6$	0.005	Ns/m

Table 2: Modified Super-Twisting Controller Parameters.

Orientation gains	Value	Position gains	Value
$k_{1\phi}$	10.0	k_{1x}	1.5
$k_{2\phi}$	7.5	k_{2x}	3.0
$k_{3\phi}$	5.0	k_{3x}	1.5
$k_{4\phi}$	3.5	k_{4x}	1.5
$k_{1\theta}$	10.0	k_{1y}	2.0
$k_{2\theta}$	7.5	k_{2y}	4.0
$k_{3\theta}$	5.0	k_{3y}	1.5
$k_{4\theta}$	3.5	k_{4y}	1.5
$k_{1\psi}$	10.0	k_{1z}	5.0
$k_{2\psi}$	7.5	k_{2z}	3.5
$k_{3\psi}$	5.0	k_{3z}	2.5
$k_{4\psi}$	3.5	k_{4z}	1.5

Table 3: High Order Sliding Mode Observer parameters.

Parameter	Value
λ_{1x}	6.75
λ_{2x}	30.00
λ_{3x}	6.75
λ_{4x}	1.50
λ_{1y}	6.75
λ_{2y}	30.00
λ_{3y}	6.75
λ_{1z}	5.00
λ_{2z}	1.00
λ_{3z}	10.00
λ_{4z}	1.30

Super-Twisting Controller and for the High Order Sliding Mode Observer, respectively.

Figure 2 shows the position of the Quadrotor in the $X - Y$ plane when a square reference is tracked. The upper graph shows the performance when disturbances are not estimated by observer (3) and compensated in the control law It can be observed the notable degradation in the performance of the vehicle generated by the external disturbances. The lower graph shows the trajectory of the UAS when the external disturbances are estimated and compensated, a significant improvement in the tracking is appreciated.

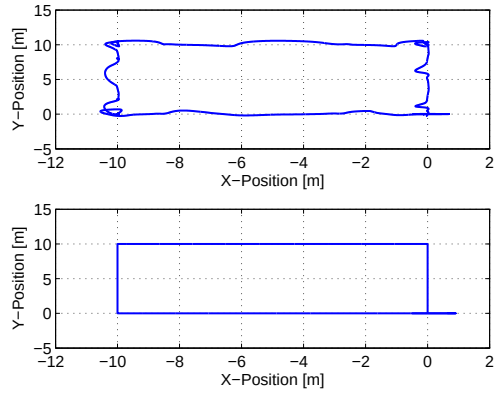

Fig. 2: Square trajectory tracking. Upper graph shows the performance without disturbance compensation. Lower graph presents the performance with disturbance compensation.

The trajectories tracking for X-axis and Y-axis without disturbances compensation are show in Figure 3. It can be appreciated that the tracking performance is affected by external disturbances, resulting in the degradation of the UAS behavior shown in upper graph of Figure 2.

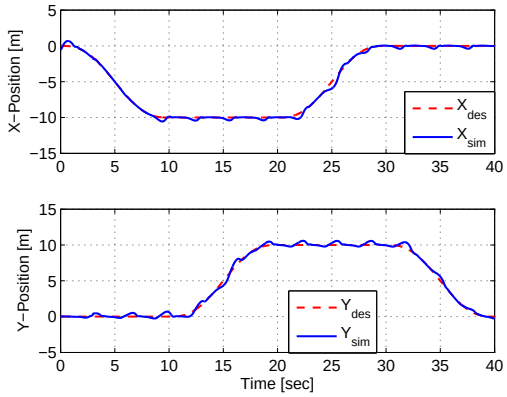

Fig. 3: Position in X-axis (upper graph) and Y-axis (bottom graph) without disturbances compensation, when the Quadrotor tracks a square reference.

Finally, Figure 4 depicts the estimation of the disturbances, which are induced to the vehicle's orientation dynamics in the form of an acceleration to simulate a more realistic situation. Notice the effectiveness of the high order sliding mode observer in the estimation of the disturbances.

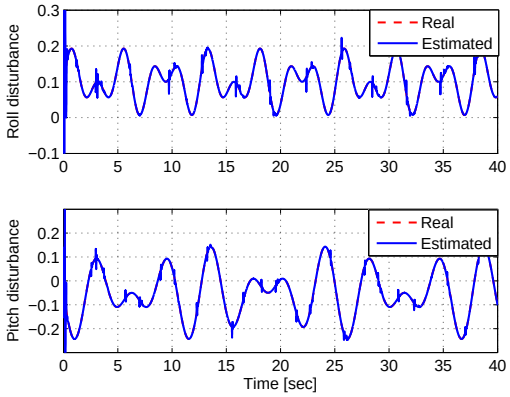

Fig. 4: Estimation of the disturbances induced on the acceleration dynamics of roll and pitch angles.

5.2 Experimental Results

In this section we present the real-time results of the proposed controller for trajectory tracking of a desired path subject to external disturbances, as well as a hovering-mode flight in order to demonstrate the good performance of this control strategy when it is applied to the Quadrotor aircraft. For the implementation of the proposed algorithms at outdoors environments we used a *Real Time Kinematic-Global Positioning System* (RTK-GPS) that provides improved location accuracy, from the $2-meters$ nominal GPS accuracy to around $3cm$ in the XY-plane. We used a *Piksi* RTK-GPS, which was designed for autonomous vehicle guidance applications, such as, formation flight and autonomous landing, GPS/GNSS research and surveying systems.

We decided to use this kind of GPS because of its effectiveness for locating an object in the 3D space (in our case, the aircraft) and because of its excellent characteristics such as the described below:

- Centimeter-accurate relative positioning (carrier phase RTK)
- $10Hz$ position/velocity/time solutions
- Open-source software and board design
- Low power consumption ($-500mW$ typical)
- USB and dual UART connectivity
- Integrated patch antenna and external antenna input

The RTK-GPS requires two Piksi receivers to achieve centimeter-level positioning, one called Rover (mounted on top of the Quadrotor aircraft) and one acting as a reference station called the Base, as can be seen in Figure 5.

We use a Quadrotor aircraft propelled by four motors fitted with 10-inch propellers. The RTK-Piksi module is enclosed within a protective carbon fiber

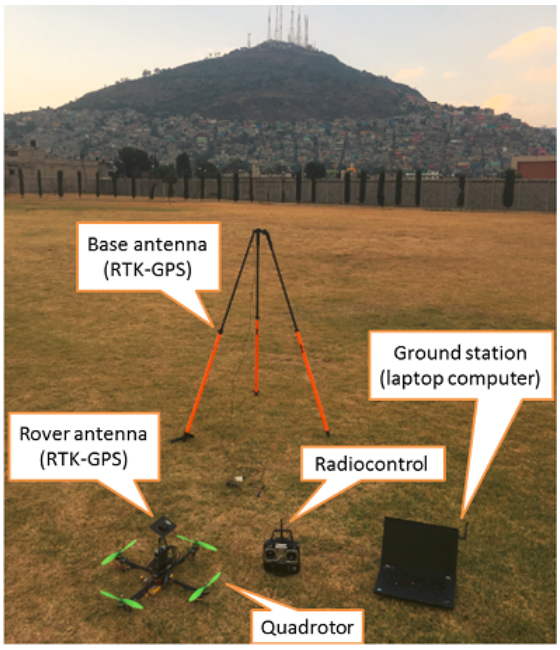

Fig. 5: The RTK-GPS setup implemented on Quadrotor aircraft.

triangle that ensures adequate operation of the RTK-GPS. The base antenna of the RTK-GPS is placed on the top of a tripod in order to obtain a better satellite reception (see Figure 5). The rover's position is sent by the Piksi module through a serial port by using the Swift Binary Protocol (SBP) which is a protocol employed for communicating with Swift devices. The SBP is read by an embedded computer (Odroid XU4) which sends to the on-board Pixhawk the 3D position measurements (X,Y,Z) obtained from the RTK module, allowing the Quadrotor aircraft to execute the trajectory tracking or performing hover-mode flight over a specific point depending on the specific escenario. Finally, we have a laptop computer as a ground station which helps us to visualize the current state of all the variables involved in the control of the aerial vehicle when the programmed task is executed. It also allows to see if there is good reception of the GPS signal in the RTK module.

In the following sections we present the obtained results of four experiments performed In order to prove the effectiveness of the proposed controller,

- Experiment 1: Hovering-mode test
- Experiment 2: Line trajectory-tracking test
- Experiment 3: Square trajectory-tracking test
- Experiment 4: Circular trajectory-tracking test

5.2.1 Hovering-mode test

This experiment was conducted for performing flight in stationary mode in the cartesian X-Y plane. Initial conditions were set for the Quadrotor aircraft positions as $x_d = 0\,m$ and $y_d = 0\,m$. Figure 6 and Figure 7 show the performance of the controller while flying at stationary mode over a particular point under external disturbances. Figure 6 shows the response in hover-mode subject to small wind gusts as external perturbation. As can be seen, the control successfully takes the helicopter to the desired coordinates $(0, 0)$ and then performs flight in hover mode. Moreover, from this figure, it can be appreciated the accuracy of the hovering flight since the Quadrotor position is always inside a circle of radius of $25cm$.

On the other hand, Figure 7 illustrates the behavior of the positions on the X and Y axes, respectively. It can be seen that these variables are maintained satisfactorily close to the given references (in our case the coordinates $(x, y) = (0, 0)$). For example, at time instants $t = 2s$ and $t = 3s$ on the X-Y axes (respectively) the Quadrotor suffers a disturbance due to a gust of wind, then the control compensates this disturbance in both axes returning the aerial vehicle to the given reference. We can conclude the proper operation of the RTK-GPS for this type of applications under moderated weeather conditions.

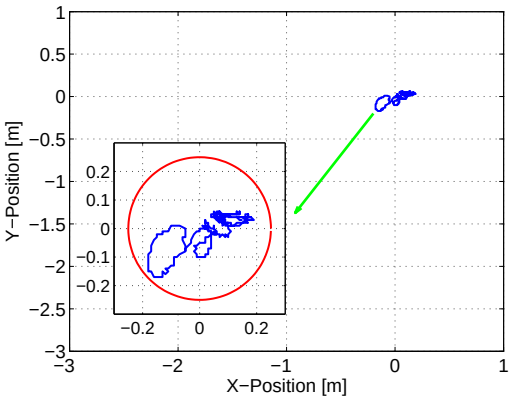

Fig. 6: Best tuning for hover at $(0, 0)$

5.2.2 Line trajectory-tracking test

In this experiment, the Quadrotor aircraft performs two specific paths (lines) during the trajectory-tracking stage. Figure 8 and Figure 9 depict the position and velocity of the aerial vehicle in the X-axis in order to demonstrate the effectiveness controller to follow the desired trajectory. We used different trajectories for each experiment described by the following parametric equations

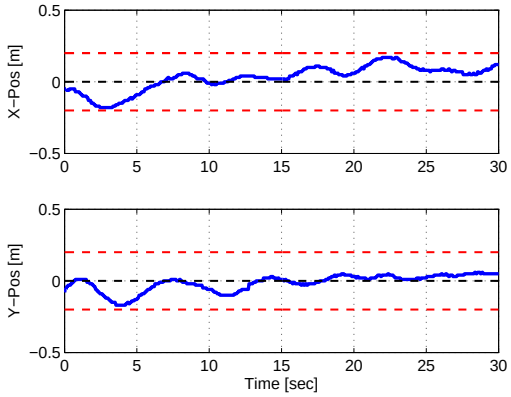

Fig. 7: Quadrotor's position in X-axis and Y-axis for Hover experiment.

[34]

$$x\left(t\right) = p_f \left[10\left(\frac{t}{t_f}\right)^3 - 15\left(\frac{t}{t_f}\right)^4 + 6\left(\frac{t}{t_f}\right)^5\right]$$
$$\dot{x}\left(t\right) = p_f \left[30\left(\frac{t^2}{t_f^3}\right) - 60\left(\frac{t^3}{t_f^4}\right) + 30\left(\frac{t^4}{t_f^5}\right)\right],$$

where $x(t)$ is the position and $\dot{x}(t)$ is the velocity of the Quadrotor aircraft at time t, respectively. Whereas p_f is the final position (length of the path) and t_f is the total route time. The following initial conditions are considered to generate the trajectory of the line: $(x, \dot{x}) = (0, 0)$. As can be seen in Figure 8, the Quadrotor aircraft starts the track-line at $t = 0s$, and completes the track-line 20 seconds later with a total distance of 20 meters travelled. Also in the same figure you can observe the behavior of the velocity profile programmed in the aerial vehicle in order to properly perform the desired path. In both graphs of the Figure 8, it is possible to clearly observe the good performance of the controller to execute the tracking of the desired path (line) under external disturbances such as wind gusts.

On the other hand, Figure 9 shows the results of position and velocity obtained from the experiment in real-time for trajectory-tracking of a line of 30 meters. As in the previous case, we can observe an excellent performance of the proposed control strategy due to the fact that even if there are disturbances such as wind gusting, the vehicle manages to follow in an adequate way the trajectory given by the parametric equation described above As well as the given velocity profile. Notice that the position and velocity obtained from the performed experiments are very similar.

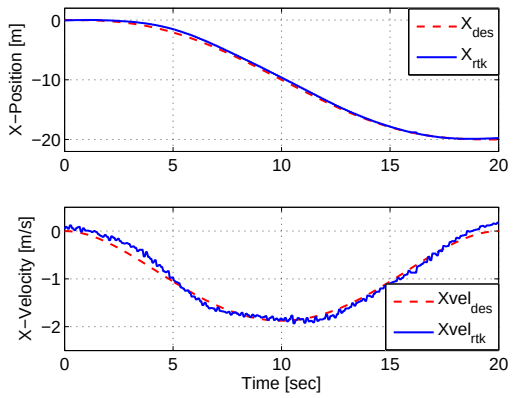

Fig. 8: Position and velocity of the UAS in X-axis. Tracking a signal reference in a distance of -20 meters from the origin.

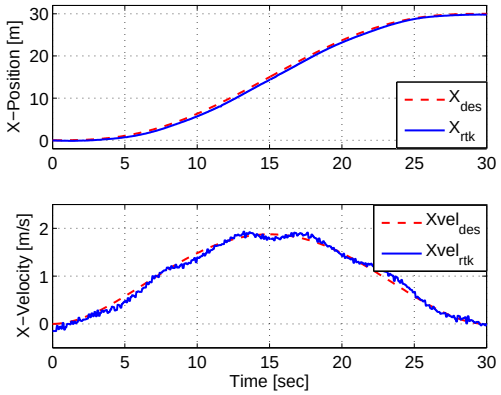

Fig. 9: Position and velocity of the UAS in X-axis. Tracking a signal reference in a distance of 30 meters from the origin.

5.2.3 Square trajectory-tracking test

For this experiment, the aerial vehicle has the task of performing a square-shaped trajectory. Figure 10 and Figure 11 show in detail the trajectory tracking of a square reference with disturbances induced by the gust of wind present in the moment of carrying out the testing at outdoors environments.

From Figure 10 a good performance of the controller can be observed since the vehicle satisfactorily followed the desired trajectory (square) under external perturbations. Also, it can be clearly seen that in the upper-left and lower-right corners of the square-trajectory there exists small deviations due to the induction of perturbations caused by the gust of wind that occurred at

that moment of the testing. While the efficiency of the control algorithm implemented in the Quadrotor aircraft for following the desired square-trajectory can be seen in Figure 10 and Figure 11, one can observer the excellent tracking performance of the proposed controller based on RTK-GPS system for X-axis and Y-axis, respectively.

In addition, the different instants in which the control signal (PWM) efficiently compensates for disturbances affecting the aerial vehicle while executing the desired square-trajectory are appreciated. A clear example of the above occurs on the Y-axis at the instant of time $t = 30\,s$, shown in Figure 11, where the control signal reacts quickly to reject the effect of the disturbance on the Quadrotor aircraft. Finally, the control signals in roll and pitch for the square trajectory tracking experiment are presented in Figure 12.

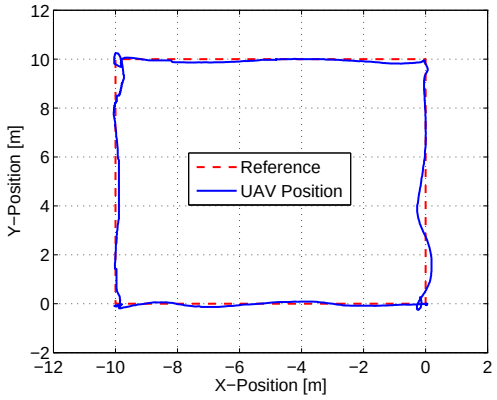

Fig. 10: Real-time experiment of trajectory tracking of a square of 10-meter .

5.2.4 Circular trajectory-tracking test

In Figure 13 and Figure 14 the experimental results for tracking a circular path are presented. The circular trajectory has a radius of 5 meters with center in the origin, with constant altitude (2 meters) and constant yaw angle (0 rad). The tracking performance in the X-Y plane can be appreciated in Figure 13 where it can be noted the behavior of the robust control strategies presented in this chapter. The references for X-axis and Y-axis that generate the circular path are shown in Figure 14. In this figure it can be appreciated the real-time position of the Quadrotor aerial vehicle in each one of the X and Y axes, where the system's behavior despite the external disturbances indicates the satisfactory performance of the designed controller. The control signals for roll and pitch angle generated to track the circular trajectory are depicted in Figure 15.

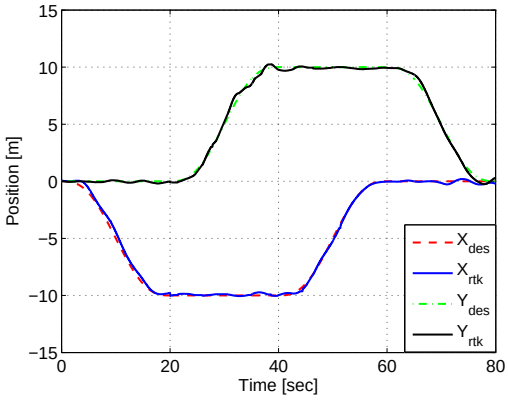

Fig. 11: Reference signal and real-time position of the Quadrotor in X-axis and Y-axis for the square trajectory tracking experiment

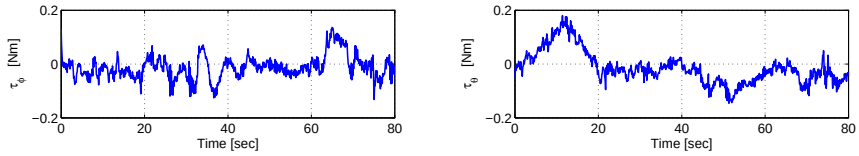

(a) Control signal in pitch.

(b) Control signal in roll.

Fig. 12: Quadrotor's control signals for X and Y axes for Square Experiment.

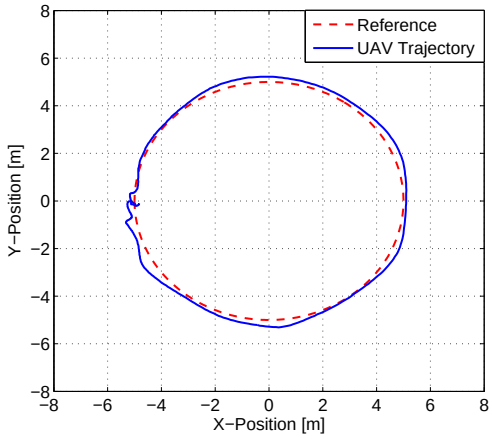

Fig. 13: Tracking performance for a circular reference trajectory in the X-Y plane

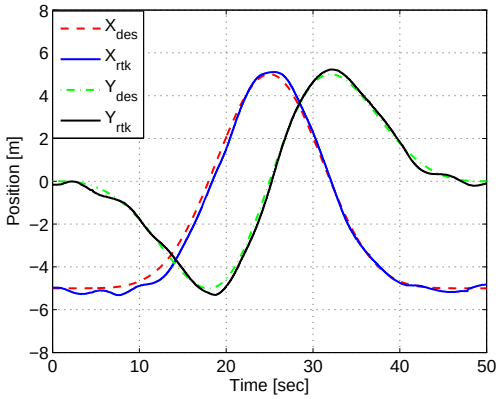

Fig. 14: Reference signal and real-time position of the Quadrotor in X-axis and Y-axis for the circular trajectory tracking experiment.

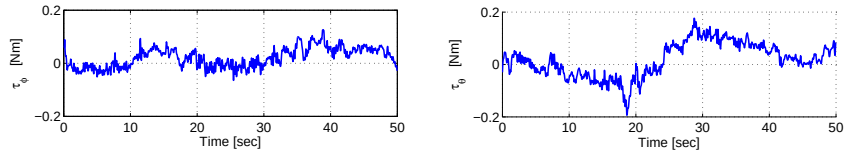

(a) Control signal in pitch. (b) Control signal in roll.

Fig. 15: Quadrotor's control signals for X and Y axes for Square Experiment.

6 Conclusions

In this paper, the Nonsingular Terminal Modified Super-Twisting Controller has been proposed for the trajectory tracking problem of an UAS type Quadrotor. To estimate the traslational velocities of the system and to improve the ability of system performance robustness, a High Order Sliding Mode Observer is employed together with the Nonsingular Terminal Controller. The Controller-Observer proposed ensures that the tracking errors converge to zero in finite-time. Finally, experimental results were obtained to show the performance of the control strategy and the experimental setup.

Acknowledgements A short version of this paper, entitled: Robust Trajectory Tracking for Unmanned Aircraft Systems Using High Order Sliding Mode Controllers-Observers, was presented in ICUAS 2017. This work was partially supported by the Mexican Secretariat of Public Education (SEP) and by the Mexican National Council for Science and Technology Project *Laboratorio Nacional en Vehículos Autónomos y Exoesqueletos 281920*.

References

1. Gordon G. Parker, Daniel J. Segalman, Rush D. Robinett. Decentralized sliding mode control for flexible link robots. Journal of Intelligent and Robotic Systems. **17**(1), 61-79 (1996)
2. Eduardo Espinoza, Octavio Garca, Israel Lugo et al. Modeling and Sliding Mode Control of a Micro Helicopter-Airplane System. Journal of Intelligent and Robotic Systems. **71**(1), 469-486 (2014).
3. S.V. Emelyanov, S.K. Korovin, and L.V. Levantovskiy. Higher order sliding modes in the binary control systems. Soviet Physics, **31**(4), 291-293 (1986).
4. W. Perruquetti and J.P. Barbot. Sliding Mode Control in Engineering, Automation and Control Engineering, CRC Press, New York (2002).
5. C. Edwards, E. Fossas Colet, and L. Fridman. Advances in Variable Structure and Sliding Mode Control, Lecture Notes in Control and Information Sciences, Springer, Berlin, Germany (2006).
6. L. Luque-Vega, B. Castillo-Toledo, Alexander G. Loukianov. Robust block second order sliding mode control for a quadrotor. Journal of the Franklin Institute. **349**(2), 719-739 (2012).
7. Lenaick Besnard, Yuri B. Shtessel, Brian Landrum. Quadrotor vehicle control via sliding mode controller driven by sliding mode disturbance observer. Journal of the Franklin Institute. **349**(2), 658-684 (2012).
8. En-Hui Zheng, Jing-Jing Xiong, Ji-Liang Luo. Second order sliding mode control for a quadrotor UAV. ISA Transactions. **53**(4), 1350-13564 (2014).
9. Diego Mercado, Pedro Castillo, R Castro, Rogelio Lozano. 2-Sliding Mode Trajectory Tracking Control and EKF Estimation for Quadrotors. 19th IFAC World Congress, Cape Town, South Africa, 8849-8854 (2014).
10. Alireza Modirrousta, Mahdi Khodabandeh. A novel nonlinear hybrid controller design for an uncertain quadrotor with disturbances. Aerospace Science and Technology. **45**, 294-308 (2015).
11. Z. Weidong, Z. Pengxiang, W. Changlong et al. Position and attitude tracking control for a quadrotor UAV based on terminal sliding mode control. 34th Chinese Control Conference, Hangzhou, China, 3398-3404 (2015).
12. I. González-Hernández, S. Salazar and R. Lozano. Robust trajectory-tracking control design for a small Quad-rotor aircraft via sliding modes. 2016 American Control Conference (ACC), Boston MA, USA, 2271-2276 (2016).
13. H.J. Jayakrishnan. Position and Attitude control of a Quadrotor UAV using Super Twisting Sliding Mode, IFAC-PapersOnLine 4th IFAC Conference on Advances in Control and Optimization of Dynamical Systems, Tiruchirappalli, India, **49**(1), 284-289 (2016).
14. Jaime A. Moreno. A Lyapunov approach to output feedback control using second-order sliding modes. IMA Journal of Mathematical Control and Information, **29**(3), 291-308 (2012).
15. F. Muñoz, M. Bonilla, I. González-Hernández et al. Super Twisting vs Modified Super Twisting algorithm for altitude control of an Unmanned Aircraft System. 12th International Conference on Electrical Engineering, Computing Science and Automatic Control (CCE), Mexico City, Mexico, 1-6 (2015).
16. Yang, Y., Qin, S., and Jiang, P. A modified super-twisting sliding mode control with inner feedback and adaptive gain schedule. International Journal of Adaptive Control and Signal Processing, **31**(3), 398-416 (2016).
17. Yi Yang and Shiyin Qin. A new modified super-twisting algorithm with double closed-loop feedback regulation. Transactions of the Institute of Measurement and Control, 1-10 (2016).
18. Yong Fhen, Xinghuo Yu, Fengling Han. On nonsingular terminal sliding-mode control of nonlinear systems. Automatica. **49** 1715-1722 (2013)
19. Mou Chen, Qing-Xian Rong-Xin Cui. Terminal sliding mode tracking control for a class of SISO uncertain nonlinear systems. ISA Transactions. **52**, 198-206 (2013).
20. Lin Xhao, Jinpeng Yu, Chong Li et al. Distributed adaptive fixed-time consensus tracking for second-order multi-agent systems using modified terminal sliding mode. Applied Mathematics and Computation. **312**, 23-35 (2017).

21. Zhenglong Zhu, Ye Yan. Space-based line-of-sight tracking control of GEO target using nonsingular terminal sliding mode. Advances in Space Research. **54**(1), 1064-1076 (2014)
22. Jun Yang, Shihua Li, Jinya Su et al. Continuous nonsingular terminal sliding mode control for systems with mismatched disturbances. Automatica. **49**(7), 2287-2291 (2013).
23. Minh-Duc Tran, Hee-Jun Kang. Nonsingular Terminal Sliding Mode Control of Uncertain Second-Order Nonlinear Systems. Mathematical Problems in Engineering. **2015**, 1-8 (2015).
24. T. Madani, B. Daachi, K. Djouani. Non-singular terminal sliding mode controller: Application to an actuated exoskeleton. Mechatronics. **33**, 136-145 (2016).
25. Arie Levant. Higher order sliding modes, differentiation and output-feedback control. International Journal of Control. **76**(9-10), 924-941 (2003).
26. A. Benallegue, A. Mokhtari, L. Fridman. High order sliding mode observer for a quadrotor UAV. International Journal of Robust and Nonlinear Control. **18**(4-5), 427-440 (2008).
27. Héctor Ríos, Jorge Davila, Leonid Fridman. High-order sliding mode observers for nonlinear autonomous switched systems with unknown inputs. Journal of the Franklin Institute. **349**(10), 2975-3002 (2012).
28. Arie Levant. Homogeneity approach to high-order sliding mode design. Automatica. **41**(5), 823-830 (2005).
29. Jaime A. Moreno. Lyapunov function for Levant's Second Order Differentiator. 51st IEEE Conference on Decision and Control (CDC), Maui Hawai, USA, 6448-6453 (2012).
30. Jaime A. Moreno and M. Osorio. A Lyapunov approach to second-order sliding mode controllers and observers. 47th IEEE Conference on Decision and Control (CDC). Cancun, Mexico, (2856-2861) 2008.
31. Michael Defoort and Mohamed Djemai. A Lyapunov-based design of a modified supertwisting algorithm for the Heisenberg system. IMA Journal of Mathematical Control and Information. **30**(2), 185-204 (2013).
32. Sylvain Bertrand, Nicolas Gunard, Tarek Hamel et al. A hierarchical controller for miniature VTOL UAVs: Design and stability analysis using singular perturbation theory. Control Engineering Practice. **19**(10), 1099-1108 (2011).
33. Hao Liu,Yongqiang Bai, Geng Lu et al. Robust Tracking Control of a Quadrotor Helicopter. Journal of Intelligent and Robotic System. **75**(3-4), 595-608 (2014).
34. Mizoshita Y, Hasegawa S and Takaishi K. Vibration minimized access control for disk drives. *IEEE T. Magn.* 1996; 32(3): 1793?1798.